small crystals between copper electrodes was constructed, which allowed the crystals to be monitored during measurements. An atmosphere of 1–2 bar SF_6(g) was used, and conductivity measurements (Keithley electrometer 6517A) were performed on six single crystals of TPP · $y(I_2)$ ($y \approx 0.65$–0.75, $T = 25\,^{\circ}C$), which were obtained from two different crystallization attempts (route III, Figure 3). $\sigma_{\parallel}$ values in the order of 10^{-6}–$10^{-8}\ \Omega^{-1}\,m^{-1}$ were found for a potential of 50 V. However, three of these crystals were exposed to a voltage of 50 V, an increase in the current I (up to a factor of two) was observed with time. In cases where the voltage was 500–1000 V, the conductivity could be enhanced by a factor of 30–300, depending on the individual crystals. For crystals in which a stable current was established after several hours, an anisotropy factor ($\sigma_{\parallel}$, $\sigma_{\perp}$) of about 30 was measured. This factor provides evidence for a preferred conductivity along I_2 chains in the TPP channels. Further investigation of the nonlinearity and the time dependence of the $I(U)$ function is in progress.

In summary, we present the first example of I_2 molecules being brought into a chainlike configuration, surrounded by a π-donor-type environment, which separates chains laterally. Observed values of the conductivity of TPP · $y(I_2)$ are of the same order as those in the (b,c) plane[11] of iodine ($1.7 \times 10^{-6}\ \Omega^{-1}\,m^{-1}$, 25 °C). Efficient sorption of I_2 by the TPP · x(THF) zeolite crystals may find application in the sensing and removal of radioactive $^{129}I_2$.[19]

Experimental Section

^{1}H NMR spectra were recorded on a Bruker-Spectroscopin AC 300 spectrometer. The UV/Vis spectra were measured on a Cary spectrometer.

Preparation of TPP: Hexachlorocyclophosphazene (recrystallized in heptane), sublimed pyrocatechol, and anhydrous sodium carbonate were mixed in dry THF. The resulting precipitate was filtered off and dried. The product was purified by recrystallization (toluene) and a double sublimation ($p = 10^{-2}$ mbar, $T = 210\,^{\circ}C$).

Preparation of the TPP · x(THF) clathrate: TPP was dissolved in THF at 60 °C. Single crystals up to several millimeters long were obtained by slow cooling (1 °C h^{-1}). The ratio of TPP/THF was determined by ^{1}H NMR spectroscopy ($x \approx 0.60$, Ia). Partially desolvated clathrate crystals were obtained when exposed to vacuum at room temperature for 24 h ($x \approx 0.35$, Ib).

Preparation of inclusion compounds TPP · x'(THF) · $y(I_2)$ (route I): TPP · x(THF) crystals were sealed in ampoules ($V \approx 3$ cm^3) with an excess of iodine and placed into the homogeneous hot zone of a glass oven at a temperature of 25–100 °C.

Preparation of inclusion compounds TPP · $y(I_2)$, route II: Cocrystallization was performed in the gas phase in ampoules ($V \approx 3$ cm^3), up to 180 °C, with a small temperature gradient between iodine(l) and TPP(s).

Route III: Sublimated TPP and an excess of iodine were dissolved in mesitylene at 80–100 °C. Black single crystals (III), were obtained by slow cooling (1 °C h^{-1}). The ratio of TPP/iodine was measured by UV/Vis spectroscopy, by using three independent series of crystals and standard solutions for iodine. The average content (y) of I_2 varied between 0.65–0.75 for different batches. A value of $y = 0.75$ demonstrates that batches with a maximum concentration of iodine could be prepared.

Received: January 2, 2002 [Z18461]

[1] C. Joachim, S. Roth, *Atomic and Molecular Wires*, Kluwer Academic, Dordrecht, **1997**.
[2] K. J. Donovan, E. G. Wilson, *Synth. Met.* **1989**, *28*, 569–574.
[3] C. H. Olk, J. P. Heremanns, *J. Mater. Res.* **1994**, *9*, 927–932.
[4] R. Wiesendanger, H.-J. Güntherrodt, *STM I, II, Springer Series in Surface Sciences 20, 28*, Springer, Berlin, **1992**.
[5] B. Ye, M. L. Trudeau, D. M. Antonelli, *Adv. Mater.* **2001**, *13*, 561–565.
[6] D. Brühwiler, N. Gfeller, G. Calzaferri, *J. Phys. Chem. B* **1998**, *102*, 2923–2929.
[7] H. R. Allcock, *J. Am. Chem. Soc.* **1964**, *86*, 2591–2595.
[8] H. R. Allcock, L. A. Siegel, *J. Am. Chem. Soc.* **1964**, *86*, 5140–5144.
[9] L. A. Siegel, J. H. van der Hende, *J. Chem. Soc. A*, **1967**, 817–820.
[10] P. Sozzani, A. Comotti, R. Simonutti, T. Meersmann, J. W. Logan, *Angew. Chem.* **2000**, *112*, 2807–2810; *Angew. Chem. Int. Ed.* **2000**, *39*, 2695–2699.
[11] A. S. Balchin, H. G. Drickamer, *J. Chem. Phys.* **1961**, *34*, 1948–1949.
[12] G. DeBoer, J. W. Burnett, M. A. Young, *Chem. Phys. Lett.* **1996**, *259*, 368–375.
[13] M. Noltemeyer, W. Sänger, *Nature* **1976**, *259*, 629–632; M. Noltemeyer, W. Sänger, *J. Am. Chem. Soc.* **1980**, *102*, 2710–2713; R. D. Bailey, G. W. Drake, M. Grabarczyk, T. W. Hanks, L. L. Hook, W. T. Pennington, *J. Chem. Soc. Perkin Trans. 2* **1997**, *12*, 2773–2779; F. H. Herbstein, M. Kapon, G. M. Reisner, *Acta Crytallogr. Sect. B* **1985**, *41*, 348–354; M. Chachisvilis, I. Garcia-Ochoa, A. Douhal, A. H. Zewail, *Chem. Phys. Lett.* **1998**, *29*, 153–159.
[14] M. Kočiřik, J. Kornatowski, V. Masařik, P. Novák, A. Zikánová, J. Maixner, *Microporous Mesoporous Mater.* **1998**, *23*, 295–308; G. Wirnsberger, H. P. Fritzer, A. Popitsch, G. van der Goor, P. Behrens, *Angew. Chem.* **1996**, *108*, 2951–2953; *Angew. Chem. Int. Ed. Engl.* **1996**, *35*, 2777–2779.
[15] T. Hertzsch, S. Kluge, F. Budde, E. Weber, J. Hulliger, *Adv. Mater.* **2001**, *13*, 1864–1867.
[16] G. Kaupp, M. Haak, *Angew. Chem.* **1996**, *108*, 2948–2951; *Angew. Chem. Int. Ed. Engl.* **1996**, *35*, 2774–2777.
[17] J. Joens, *J. Org. Chem.* **1989**, *54*, 1126–1128.
[18] H. R. Allcock, M. L. Levin, R. R. Whittle, *Inorg. Chem.* **1986**, *25*, 41–47.
[19] J. Hulliger, T. Herzsch, patent application, USA, **2001**.

Trapping Energy from and Injecting Energy into Dye–Zeolite Nanoantennae**

Huub Maas and Gion Calzaferri*

The light-harvesting system in green plants is a supramolecular machine that collects light energy for photosynthesis. The beauty of this photonic antenna has inspired many researchers to examine and even try to mimic it. Different approaches have been used to build artificial photonic antennae.[1–5] Exciting results based on a host–guest system have been obtained in our group[6–10] with the host material zeolite L, a hexagonal crystal with one-dimensional channels

[*] Prof. Dr. G. Calzaferri, Dipl.-Chem. H. Maas
Department of Chemistry and Biochemistry
University of Berne
3012 Berne (Switzerland)
Fax: (+41) 31-631-3994
E-mail: Gion.Calzaferri@iac.unibe.ch

[**] This work is part of the Swiss National Science Foundation Project NFP 47 (4047-057481). We thank René Bühler for the synthesis of the zeolite L nanocrystals.

  1433-7851/02/4113-2284 $ 20.00+.50/0

along the crystal axis.[11–13] As guests we have used a wide range of highly fluorescent dye molecules. The size and shape of these dyes is such that they can enter the free open diameter of the zeolite L channels but they are prevented from forming dimers once inside. In this way we are able to build highly organized systems in which monomeric dyes are present in a high concentration. The distance between the individual dye molecules is in the order of magnitude of the Förster radius for energy transfer,[14] which enables efficient energy transport in such dye-loaded zeolite L crystals. We have made photonic antennae with two (see Figure 1 A)[7] and three dyes,[9] and inverse antennae in which the donors are located at both ends of the crystals and the acceptors in the middle.[15]

The systems reported so far are able to transport electronic excitation energy radiationless within the zeolite crystal structure. To mimic the natural supramolecular machine and for a number of technologically interesting applications it would be desirable to lead the collected energy out of the crystals, or to inject energy from the exterior into the dye-loaded crystals. Our suggestions to reach this goal involve stopcock molecules (as shown in Figure 1 B).[6, 16] These molecules have a stopcock shape with a head that is too big to penetrate the free open diameter of the zeolite channels and a label that is smaller and can enter. The head and the label are connected by a flexible spacer. Herein we show for the first time that such stopcocks can trap electronic excitation energy at the zeolite crystal surface, and inject excitation energy into dye-loaded zeolite L crystals in a complementary arrangement.

The ratio between the internal and the external surface of the zeolite L crystals is proportional to the ratio between the number of molecules that can be inserted in the crystal channels and the number of molecules that can be adsorbed as a monolayer on the external surface. One way of keeping this ratio small is by using small zeolite L crystals; the synthesis of zeolite L crystals with a size of about 30 nm has been reported.[7, 17] The large external surface of these nanocrystals makes them suitable hosts to show energy transfer from molecules inside the crystals to molecules on the surface and vice versa.

Because the zeolite L crystals have a cylindrical shape, one can distinguish between two external surfaces: the coat, and the base. The coat is vaulted and lacks channel entrances, while the base is flat and contains the channel entrances. These differences give rise to different adsorption affinities.

Scheme 1 shows the dye molecules BTRX and B493/503 we have used as stopcocks. Their head consists of a BODIPY fluorophore, and their label is a succinimidyl ester.[18] The succinimidyl ester makes the label polar and we know that keto groups form specific interactions to sites inside the channels. Although BTRX and B493/503 have polar groups it is possible to dissolve small amounts in an apolar solvent such as cyclohexane. If a suspension of nanocrystals in the same solvent is then added to this solution, the stopcocks are extracted from the solution onto the polar zeolite surface.

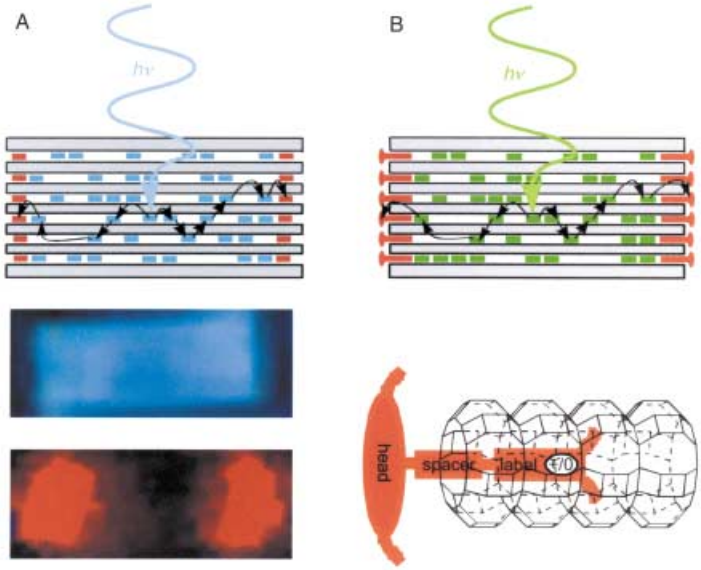

Figure 1. Dye-loaded zeolite L antenna; A) blue-emitting donor molecules inside the zeolite transfer electronic excitation energy to red-emitting acceptor molecules at the left and right of the cylindrical crystal. B) Antenna system with stopcock molecules as external traps and a schematic picture of a stopcock at the end of a zeolite L channel. The stopcock contains a head, a spacer, and a label.

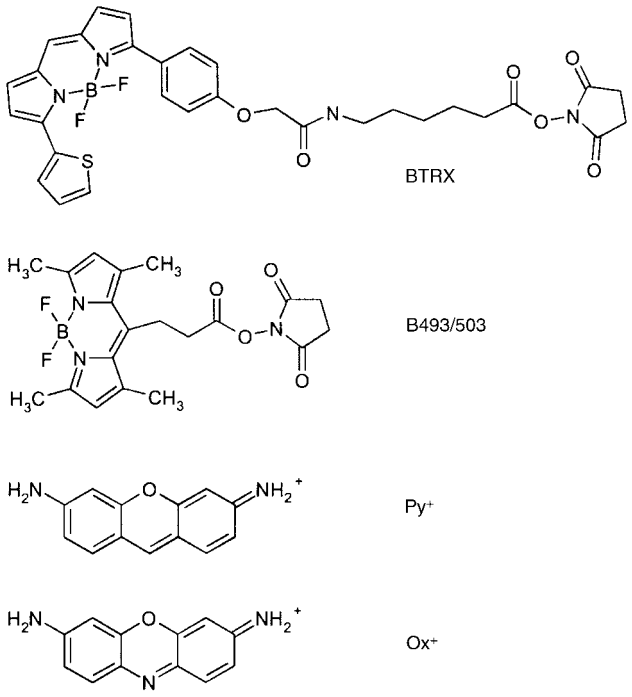

Scheme 1. Dyes examined: BODIPY TR-X SE (BTRX), BODIPY 493/503 SE (B493/503), pyronine$^+$ (Py$^+$), and oxonine$^+$ (Ox$^+$).

Owing to the adsorption equilibrium, the more preferred adsorption sites will after some time be predominantly occupied. Thus a difference in adsorption affinity between the coat and the base of the crystals will be pronounced after the adsorption process has reached its equilibrium state. If the dye concentration on the crystal surface becomes too high, aggregation will occur. Aggregates usually quench fluorescence[19] and it is therefore necessary to work with well-controlled amounts of dye so that only monomers are present.

  1433-7851/02/4113-2285 $ 20.00+.50/0

Energy-transfer experiments were done on the two different systems shown in Figure 2. The Py^+/BTRX system was used to investigate energy transfer from Py^+ molecules inside the zeolite channels to the BTRX stopcocks, and the Ox^+/B493/503 system to investigate energy transfer from B493/503 stopcocks to Ox^+ molecules inside the zeolite channels. For these experiments zeolite nanocrystals with a size of about 30 nm were used.

The optical properties of Py^+-loaded and of BTRX modified nanocrystals are shown in Figure 3 A. The spectral overlap integral between the fluorescence spectrum of Py^+ and the excitation spectrum of BTRX is large—a prerequisite for effective energy transfer. Py^+ – zeolite L crystals with different occupational probabilities, p_{Py}, were modified with two BTRX stopcocks per channel. Py^+ was selectively excited at 22000 cm^{-1}. Figure 3 B shows the resulting fluorescence spectra for different Py^+ loads. After Py^+ excitation, we can clearly see the fluorescence band of BTRX around 16000 cm^{-1}. It is the result of energy transfer from Py^+ molecules inside the crystals to BTRX molecules on the external surface (Figure 2 top). The dotted spectrum in Figure 3 B arises from a sample in which the amount of Py^+ inside the channels is twice the amount of BTRX on the external surface. An increase of the donor concentration leads to a decrease of the mean donor – acceptor and mean donor – donor separation. It is expected that this results in more effective energy transfer, which is what we observe (Figure 3 B). We attribute the bathochromic shift of the Py^+ emission band to self-absorption and re-emission.[8]

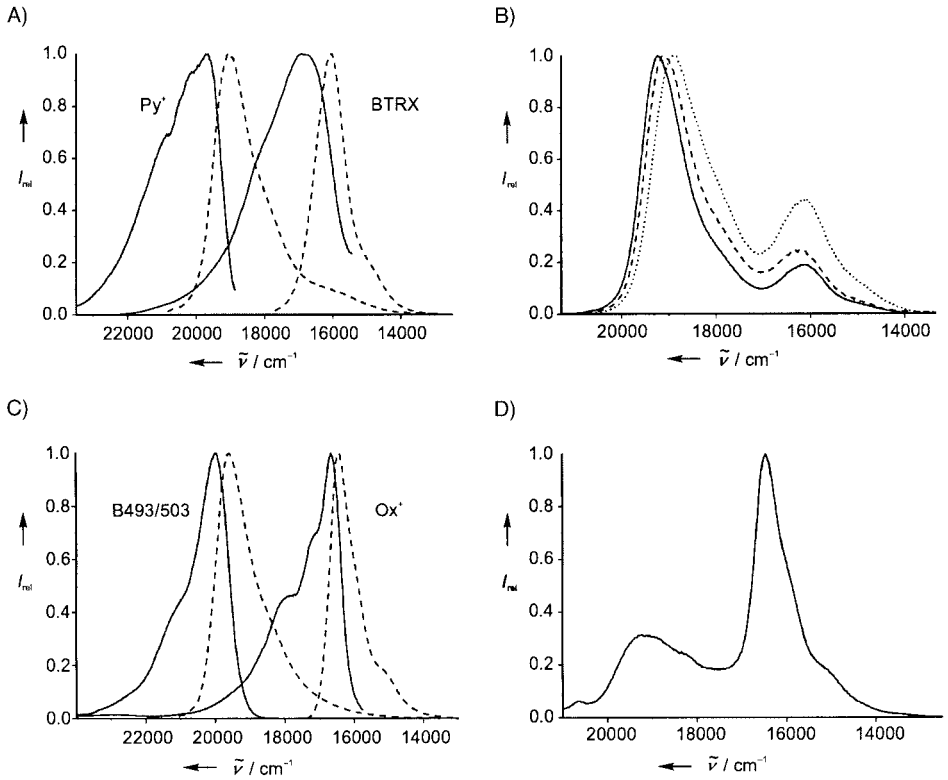

Figure 3. A) Fluorescence (– – –) and fluorescence excitation (——) spectra of Py^+ in, and BTRX on the external surface of zeolite L nanocrystals; ε_{Py^+} (λ_{max}) $\approx$ 83200 $cm^{-1}M^{-1}$, ε_{BTRX} (λ_{max}) $\approx$ 68000 $cm^{-1}M^{-1}$; $J_{Py^+\text{-}BTRX} = 3 \times 10^{-10}$ cm^3M^{-1}, $p_{Py} = 0.06$; the crystals with BTRX were modified with two molecules per channel. B) Fluorescence spectra of Py^+-zeolite L nanocrystals modified with two BTRX per channel. ——: $p_{Py} = 0.02$, – – –: $p_{Py} = 0.06$, - - - -: $p_{Py} = 0.10$. C) Fluorescence (– – –) and fluorescence excitation (——) spectra of Ox^+ in, and of B493/503 on the external surface of zeolite L nanocrystals; ε_{Ox^+} (λ_{max}) $\approx$ 84100 $cm^{-1}M^{-1}$, $\varepsilon_{B493/503}$ (λ_{max}) $\approx$ 84000 $cm^{-1}M^{-1}$; $J_{B493/503\text{-}Ox^+}$ 1.5×10^{-10} cm^3M^{-1}, $p_{ox} = 0.008$; the crystals with B493/503 were modified with one molecule per channel. D) Fluorescence spectra of Ox^+-zeolite L nanocrystals modified with one B493/503 per channel. All spectra have been scaled to the same height $I_{max} = 1$.

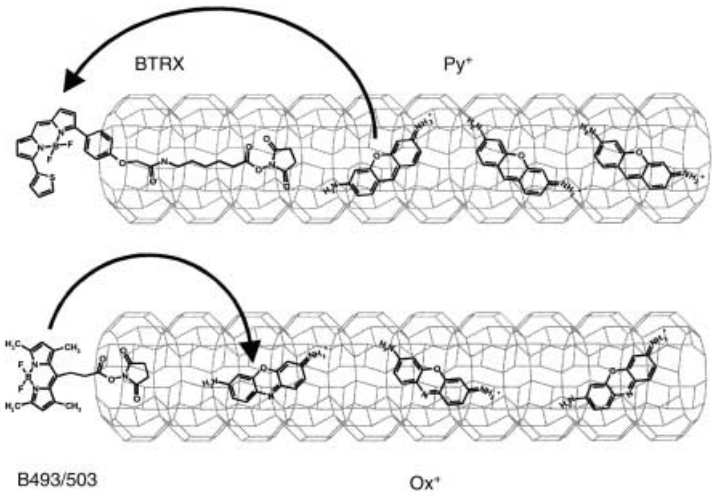

Figure 2. Top: Py^+-filled zeolite L channels; the ends of the channels are modified with BTRX stopcocks for external trapping of electronic excitation energy. Bottom: Ox^+-filled zeolite L channels; and the ends of the channels are modified with B493/503 stopcocks for electronic excitation energy injection.

The reverse of this external trapping is injection of electronic excitation energy. For this, we need a system, such as the chosen B493/503-modified Ox^+-zeolite L, in which the donor stopcocks are at both ends and the acceptor molecules are inside the zeolite channels (Figure 2 bottom). We first characterized the Ox^+-zeolite nanocrystals and the nanocrystals modified with B493/503 separately (Figure 3 C). Again the spectral overlap integral between the emission spectrum of B493/503 and the excitation spectrum of Ox^+ is large. The B493/503 stopcocks are excited selectively at 21740 cm^{-1}. We modified Ox^+-zeolite L crystals with one molecule of B493/503 per channel. The occupational probability of Ox^+ was chosen to be very small (0.008) so that 3.5 times more donor molecules were present than acceptor molecules. After specific excitation of the B493/503 stopcocks at 21740 cm^{-1} the emission spectrum of Figure 3 D was obtained, which shows that impressive energy transfer takes place from the B493/503 stopcocks to the Ox^+ molecules. The emission band at 16000 cm^{-1} is due to energy injection from

  1433-7851/02/4113-2286 $ 20.00+.50/0 *Angew. Chem. Int. Ed.* **2002**, *41*, No. 13

B493/503. This energy injection works even better than the energy trapping of excited Py^+ molecules by BTRX. The length of the tail of BTRX is 1.8 nm and that of B493/503 is 0.9 nm. The shorter tail of B493/503 allows shorter donor–acceptor separations R_{DA}. Because the Förster energy transfer rate falls off with R_{DA}^{-6} the shorter distance is presumably the main reason for the higher transfer efficiency.

Although the nanocrystals are a good choice for energy-transfer experiments, it is at the present time technically not feasible to examine the organization of the individual dyes with an optical microscope. To visualize this we therefore used large zeolite L crystals of about 2 μm length. Our aim was to establish on which zeolite surface the stopcocks preferably bind and to try to image the energy transfer. Modification of large Py^+-zeolite L crystals with two BTRX molecules per channel led to the fluorescence microscope images shown in Figure 4. The zeolite crystals were exchanged with Py^+ for very short periods so that the Py^+ molecules could not diffuse far into the zeolite channels. This accounts for why the middle part of the crystals in Figure 4 are dark.

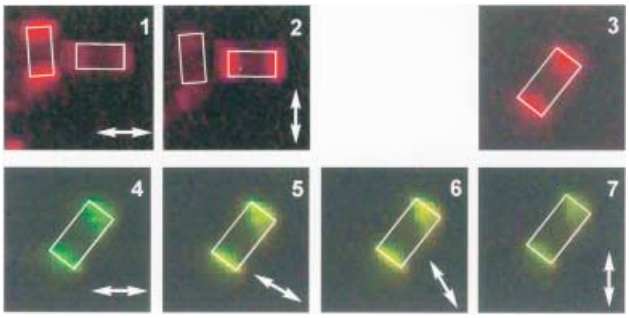

Figure 4. Fluorescence microscope images of 2 μm Py^+-zeolite L crystals modified with 2 BTRX molecules per channel. The white rectangles indicate single zeolite L crystals. 1, 2) Images of BTRX-modified zeolites after excitation at 545–580 nm and detection with a 610 nm cut-off filter using a polarizer (the direction of the transmitted polarization is indicated by the arrows); 3) image of a crystal detected without polarizer. 4–7) images of the same crystal as in 3) after excitation at 470–490 nm and detection with a 515 nm cut-off filter at different polarizations.

Images 1 and 2 in Figure 4 show the emission after BTRX excitation of two perpendicular lying crystals; the transmitted polarization direction is indicated by the arrows. It is clear that the stopcocks are located at the bottom and top of the cylindrical crystals and that the BTRX emission is polarized perpendicular to the crystal axis. The $S_0 \leftarrow S_1$ transition dipole moment of the BODIPY fluorophore is polarized along the chromophore axis.[20] Molecular orbital calculations[10c, 21] reveal that the $S_0 \leftarrow S_1$ transition dipole moment of BTRX is similarly polarized. One would therefore expect an emission perpendicular to the crystal axis when the molecules partly penetrate the zeolite L channels. Images 3–7 in Figure 4 all show the same crystal. Image 3 shows the emission after BTRX excitation and images 4–7 show the emission after Py^+ excitation. The color of the emitted light changes significantly with polarization. Depending on the polarization a green to yellow emission dominates. The yellow color is a mixture of green (Py^+) and red (BTRX) emission. If the Py^+ and the BTRX molecules are differently oriented, different contributions of red and green occur for the different polarization. For the polarization perpendicular to the crystal axis (as approximately is the case in image 5), the red contribution is largest and the crystals appear yellow.

In conclusion we have shown that electronic excitation energy can be trapped outside and injected into nanoantennae by stopcock molecules that preferably adsorb at the base of the cylindrical zeolite L crystals. This opens the door to a wide range of applications, for example, for mimicking the natural photosynthesis apparatus, for supramolecular nanoprobes, and in dye-sensitized solar cells and light-emitting diodes.[16]

Experimental Section

Chemically pure zeolite L materials were synthesized and characterized as described in reference [7]. The potassium zeolite L crystals were pretreated by stirring in a buffer of pH 6 for 1 h followed by washing with doubly distilled H_2O three times. Py^+ and Ox^+ were synthesized and purified according to the procedure in reference [10b]. BTRX (BODIPY TR-X SE) and B493/503 (BODIPY 493/503 SE) were obtained from Molecular Probes Inc. and used as received. Py^+ and Ox^+ molecules were inserted in the zeolite L channels by ion exchange from H_2O. An aqueous zeolite L suspension was treated in an ultrasonic bath for 20 min and then added to an aqueous dye solution containing the appropriate amount of dye. The mixture was refluxed for 1 h. Afterwards the dye-loaded crystals were washed twice with MeOH by ultrasonic treatment for 15 min to remove dyes from the external surface. For the adsorption of BTRX and B493/503 the zeolite L crystals were suspended in cyclohexane and sonicated for 20 min. Then a dye solution in cyclohexane with the appropriate amount of dye was added and the mixture was sonicated for 30 min at room temperature. Adsorption of BTRX and B493/503 onto the dye-loaded zeolites did not extract any cationic dyes from inside the zeolite. Solid-state samples were prepared on 16 mm diameter quartz plates for fluorescence measurements which were carried out the same day.

Fluorescence spectra were measured with a Perkin Elmer LS 50B luminescence spectrometer using suitable cut-off filters (Py^+ was excited at 455 nm and detected at 550 nm; BTRX was excited at 550 nm and detected at 690 nm; Ox^+ was excited at 560 nm and detected at 670 nm; B493/503 was excited at 460 nm and detected at 575 nm). Absorption spectra were recorded on a Perkin Elmer Lambda 900 spectrophotometer. Optical microscopy images of fluorescent samples were recorded under an Olympus BX 60 microscope combined with a Kappa CF 20 DCX Air K2 CCD camera with 100× magnification using an immersion oil. The light stemming from a mercury lamp was first passed through a 438 nm cut-off filter. It was then passed through appropriate excitation cubes comprising a narrow-band excitation filter, a dichroic mirror, and a cut-off filter. Py^+ was excited between 470 and 490 nm and detected with a cut-off filter at 515 nm, BTRX was excited between 545 and 580 nm and detected with a cut-off filter at 610 nm. By inserting a polarizer in front of the camera the fluorescence images could be examined at different polarizations.

Received: December 5, 2001 [Z18332]

[1] V. Balzani, S. Campagna, G. Denti, A. Juris, S. Serroni, M. Venturi, *Sol. Energy Mater. Sol. Cells* **1995**, *38*, 159.
[2] H. Bücher, K. H. Drexhage, M. Fleck, H. Kuhn, D. Möbius, F. P. Schäfer, J. Sondermann, W. Sperling, P. Tillmann, J. Wiegand, *Mol. Cryst.* **1967**, *2*, 199.
[3] B. A. Gregg, U. Resch, *J. Photochem. Photobiol. A* **1995**, *87*, 157.
[4] S. E. Webber, *Chem. Rev.* **1990**, *90*, 1469.
[5] V. Balzani, P. Ceroni, S. Gestermann, M. Gorka, C. Kauffmann, M. Maestri, F. Vögtle, *ChemPhysChem* **2000**, *4*, 224.
[6] G. Calzaferri, H. Maas, M. Pauchard, M. Pfenniger, S. Megelski, A. Devaux in *Advances in Photochemistry*, *Vol. 27* (Ed.: D. C. Neckers), Wiley-VCH, Weinheim, **2002**, in press.
[7] S. Megelski, G. Calzaferri, *Adv. Funct. Mater.* **2001**, *11*, 277.
[8] G. Calzaferri, D. Brühwiler, S. Megelski, M. Pfenniger, M. Pauchard, B. Hennessy, H. Maas, A. Devaux, U. Graf, *Solid State Sci.* **2000**, *2*, 421.

  1433-7851/02/4113-2287 $ 20.00+.50/0

[9] M. Pauchard, A. Devaux, G. Calzaferri, *Chem. Eur. J.* **2000**, *6*, 3456.
[10] a) N. Gfeller, G. Calzaferri, *J. Phys. Chem. B* **1997**, *101*, 1396; b) N. Gfeller, S. Megelski, G. Calzaferri, *J. Phys. Chem. B* **1999**, *103*, 1250; c) S. Megelski, A. Lieb, M. Pauchard, A. Drechsler, S. Glaus, C. Debus, A. J. Meixner, G. Calzaferri, *J. Phys. Chem. B* **2001**, *105*, 25.
[11] P. A. Anderson, A. R. Armstrong, A. Porch, P. P. Edwards, L. J. Woodall, *J. Phys. Chem. B* **1997**, *101*, 9892.
[12] C. Bärlocher, W. M. Meier, D. H. Olsen, *Atlas of Zeolite Framework Types*, Elsevier, Amsterdam, **2001**.
[13] D. W. Breck, *Zeolite Molecular Sieves*, Wiley, New York, **1974**.
[14] a) T. Förster, *Ann. Phys. (Leipzig)* **1948**, *6*, 55; b) T. Förster, *Fluoreszenz Organischer Verbindungen*, Vandenhoeck & Ruprecht, Göttingen, **1951**; c) T. Förster in *Comparative Effects on Radiation*, Wiley, New York, **1960**, pp. 300–319.
[15] M. Pauchard, S. Huber, R. Méallet-Renault, H. Maas, R. Pansu, G. Calzaferri, *Angew. Chem.* **2001**, *113*, 2921; *Angew. Chem. Int. Ed.* **2001**, *40*, 2839.
[16] G. Calzaferri, M. Pauchard, H. Maas, S. Huber, A. Khatyr, T. Schaafsma, *J. Mater. Chem.* **2002**, *12*, 1.
[17] a) M. Tsapatsis, T. Okubo, M. Lovallo, M. E. Davis, *Mater. Res. Soc. Symp. Proc.* **1995**, *371*, 21; b) M. Tsapatsis, M. Lovallo, T. Okubo, M. E. Davis, M. Sadakata, *Chem. Mater.* **1995**, *7*, 1734.
[18] R. P. Haugland, *Handbook of Fluorescent Probes and Research Products*, Molecular Probes Inc., Eugene, **2001**.
[19] a) M. Kasha, H. R. Rawls, M. A. El-Bayoumi, *Pure Appl. Chem.* **1965**, *11*, 371; b) E. G. McRae, M. Kasha, *J. Chem. Phys.* **1958**, *28*, 721.
[20] J. Karolin, L. B.- Å. Johansson, L. Strandberg, T. Ny, *J. Am. Chem. Soc.* **1994**, *116*, 7801.
[21] G. Calzaferri, R. Rytz, *J. Phys. Chem.* **1995**, *99*, 12141.

Sr_4N_3: A Hitherto Missing Member in the Nitrogen Pressure Reaction Series $Sr_2N \rightarrow Sr_4N_3 \rightarrow SrN \rightarrow SrN_2$**

Yurii Prots, Gudrun Auffermann, Michael Tovar, and Rüdiger Kniep*

In the course of our investigations on the formation and existence of diazenides of strontium,[1] we developed an analytical method for quantitative nitrogen speciation.[2] By means of this technique (carrier-gas hot extraction with a controlled temperature program), we could confirm the results of the structure determinations on SrN ($\hat{=}(Sr^{2+})_4[N^{3-}]_2[N_2^{2-}]$) and $Sr[N_2]$ ($\hat{=}(Sr^{2+})[N_2^{2-}]$). The system was calibrated by using, for example, Sr_2N[3] (the starting material of the high-pressure synthesis of diazenides).[1] In the course of our studies, it turned out that Sr_2N, synthesized at ambient pressure, often contains significant portions of diazenide which were not clearly visible by X-ray or spectroscopic investigations.[4] In principle, these experimental results would be consistent with a homogeneity range of Sr_2N towards SrN according to (partial) formation of mixed crystals $Sr_{2-x}N$ (complete miscibility in the limits $0 \le x \le 1$), although previous studies[1] had provided "no indication for homogeneity ranges" of the nitride diazenides. In fact, we now find that at lower N_2 reaction pressure (already above 1 bar), Sr_2N reacts to the hitherto "overlooked" nitride–diazenide Sr_4N_3.

Sr_4N_3, a dark gray powder with metallic luster, was synthesized in autoclaves[5] by the reaction of Sr_2N with molecular nitrogen (9 bar) at 650 °C for 6 h.[6] No impurities were detected by X-ray and neutron diffraction investigations[7] at ambient pressure nor by chemical analysis.[9] The contents of oxygen, hydrogen, and carbon were below the limits of detection. At constant reaction temperature (650 °C) and time (6 h), the diffraction pattern of Sr_4N_3 was observed up to a reaction pressure of 100 bar amongst the characteristic reflections of SrN. The lattice parameters of Sr_4N_3 and SrN, determined at ambient pressure, remained unchanged within the standard deviations.

The crystal structure of the air- and moisture-sensitive microcrystalline powder of Sr_4N_3 was solved by a combination of X-ray and neutron diffraction.[7] The observed and calculated neutron diffraction diagram, as well as the difference profile, are given in Figure 1. The crystal structure of Sr_4N_3 is depicted in Figure 2 (center) showing the close

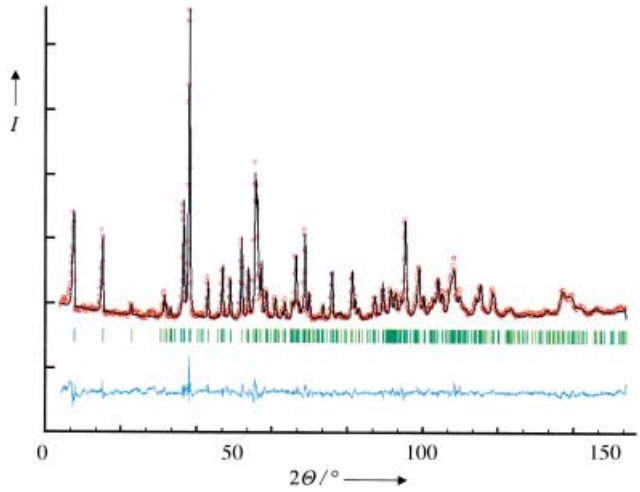

Figure 1. Neutron diffraction diagram of $Sr_4N_3 \hat{=} Sr_8[N]_4[N_2]$ (powder diffractometer E9, HMI Berlin) at 298 K: Observed (red dots), calculated (black solid line), and difference profiles (blue line). The green ticks mark the positions of the Bragg reflections of the monoclinic C-centered cell.[7]

relation to the starting material Sr_2N (left) and the next higher "pressure stage" SrN (right). The evident structural relation makes it reasonable to suppose the reaction paths during the formation of Sr_4N_3 via an intercalation step.[10] Thus, these structural chemical facts can easily be described when starting with the subnitride Sr_2N[3] as the host structure ($CdCl_2$ type). In the first step of the N_2-pressure induced intercalation which occurs already at about 1 bar (p_{N_2}), one half of the octahedral holes ($\square^{(o)}$) between two adjacent layers $^2_\infty(Sr_{6/3}N)$ along [001] in the host structure, are occupied by N_2. Thus, packages of

[*] Prof. Dr. R. Kniep, Dr. Yu. Prots, Dr. G. Auffermann
Max-Planck-Institut für Chemische Physik fester Stoffe
Nöthnitzer Strasse 40, 01187 Dresden (Germany)
Fax: (+49) 351-4646-3002
E-mail: Kniep@cpfs.mpg.de
Dr. M. Tovar
Hahn-Meitner-Institut, Berlin
Glienicker Strasse 100, 14109 Berlin (Germany)

[**] We thank the Fonds der Chemischen Industrie for financial support, the Hahn-Meitner-Institut for giving us access to the powder diffractometer E9, B. Bayer and A. Völzke for assistance with the chemical analyses.

  1433-7851/02/4113-2288 $ 20.00+.50/0